Computer Modeling in Engineering & Sciences CMES, vol.122, no.3, pp.831-862, 2020

Application of Smooth Particle Hydrodynamics Method for Modelling Blood Flow with Thrombus Formation

M. Al-Saad[1], C. A. Suarez[2, 4], A. Obeidat[2], S. P. A. Bordas[1, 2, 3, *] and S. Kulasegaram[1]

Abstract: Thrombosis plays a crucial role in atherosclerosis or in haemostasis when a blood vessel is injured. This article focuses on using a meshless particle-based Lagrangian numerical technique, the smoothed particles hydrodynamic (SPH) method, to study the flow behaviour of blood and to explore the flow parameters that induce formation of a thrombus in a blood vessel. Due to its simplicity and effectiveness, the SPH method is employed here to simulate the process of thrombogenesis and to study the effect of various blood flow parameters. In the present SPH simulation, blood is modelled by two sets of particles that have the characteristics of plasma and of platelet, respectively. To simulate coagulation of platelets which leads to a thrombus, the so-called adhesion and aggregation mechanisms of the platelets during this process are modelled by an inter-particle force model. The transport of platelets in the flowing blood, platelet adhesion and aggregation processes are coupled with viscous blood flow for various low Reynolds number scenarios. The numerical results are compared with the experimental observations and a good agreement is found between the simulated and experimental results.

Keywords: Smooth particle hydrodynamics, blood flow, thrombus, arteries, platelets.

1 Introduction

Thrombosis is considered as the most common form of haemostatic disorders, which is caused by formation of a blood clot that impedes blood flow in the vessels. Thrombus formation causes many types of diseases and conditions, such as arteriosclerosis, trauma, stroke, infarction, cancer, sepsis and others. Approximately about 70% of cardiac deaths around the globe are due to thrombosis [Panteleev, Sveshnikova, Belyaev et al. (2014)]. A thrombus is a coagulated mass of blood corpuscles that stops bleeding or atherosclerosis in arteries. In other words, a thrombus can cause a blockage of blood vessels as a result of haemostasis dysfunction. Haemostasis is considered to be a necessary reaction to prevent and stop blood loss, however the malfunctioning of a haemostatic system leads to potentially deadly accidents such as myocardial infarction

[1] School of Engineering, Cardiff University, Cardiff, CF24 3AA, UK.

[2] Department of Engineering, Institute of Computational Engineering, University of Luxembourg, Maison du Nombre, 6 Avenue de la Fonte, 4364 Esch-sur-Alzette, Luxembourg.

[3] Department of Medical Research, China Medical University Hospital, China Medical University, Taichung, Taiwan.

[4] Aix Marseille Université, CNRS, CentraleMarseille, LMA, Marseille, France.

[*] Corresponding Author: S. P. A. Bordas. Email: stephane.bordas@uni.lu.

Received: 03 September 2019; Accepted: 16 January 2020.

and ischemic stroke when the damaged arteries are the coronary or the carotids respectively [Epstein, Fuster, Badimon et al. (1992); Fuster, Badimon, Cohen et al. (1988)]. The formation of a thrombus depends on platelet activity; for example, the transport to denuded subendothelium, a formation of membrane tethers, adhesion to the subendothelium, and aggregation [Ruggeri (2003)]. Under normal blood circulation, the platelets have no propensity to adhere to the wall of the blood artery or vessels, to other cells, or to each other. Meanwhile, if the wall of a blood vessel is damaged, then platelets will rapidly adhere and accumulate on the damaged wall. Physiologically, this process of increase in the adhesiveness of platelets describes normal haemostasis; pathologically, it will cause an acute thrombosis, particularly in larger arteries, which are diseased [Begent and Born (1970)]. The aggregation of platelets and blood coagulation is considered to be an intricate process [Panteleev, Sveshnikova, Belyaev et al. (2014)]. Haemostasis can be divided into three different phases. In the first stage, the vascular phase is triggered by damage in the blood vessel wall that leads to smooth muscle contraction, thereby decreasing the diameter of the vessel in the vicinity of the damaged area. The second stage is called the platelets phase, which starts when the platelets are attached to the damaged area and is activated due to many factors such as adenosine diphosphate (ADP) and tissue characteristics. The last stage is called the coagulation phase, which can begin 30 (or more) seconds after the vessel wall is damaged [Flannery (2005)].

Platelets are considered to be one of the most important elements of the haemostasis process [Broos, Feys, De Meyer et al. (2011); Nuyttens, Thijs, Deckmyn et al. (2011)]. When an imperfection or damage is detected, the platelets react by adhering to the surface of the damaged area. The procedure of initial platelet-plug generation is called primary haemostasis. Low platelet numbers may impede the primary haemostasis and lead to death [Reininger (2008)]. Platelets are considered to be important players in primary haemostasis. They have many receptors, which can interact with subendothelial components, such as collagen, to facilitate adhesion to the damaged vessel wall [Broos, Feys, De Meyer et al. (2011); Nuyttens, Thijs, Deckmyn et al. (2011)]. During the secondary haemostasis, the accumulation of adhered platelets results in a plug, which is then further settled by, for example, fibrinogen fibres compared to the primary haemostasis [Müller (2015)]. In order to understand the mechanism of thrombosis inside the human body, thrombosis is portrayed by platelet adhesion, activation, collection and the coagulation course as shown in Fig. 1 [Wootton and Ku (1999)].

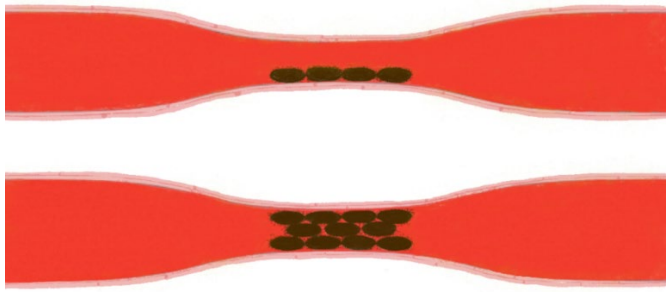

Figure 1: Thrombosis in different stages: platelet adhesion and platelet aggregation [Wootton and Ku (1999)]

As discussed above, thrombogenesis plays a crucial role in human physiological condition and it is vital to understand how thrombus formation is related to haemodynamic. As it is non-invasive and more conducive to repetitive analysis, accurate computational models provide a wide range of tools to investigate the process of thrombogenesis.

Many Eulerian-based studies have analysed the role of haemodynamic in thrombogenesis. However, these studies are limited and do not fully describe platelets motion and their behaviour. A continuum model of platelet aggregation to analyse platelet-mediated thrombogenesis, while considering platelet transport activation by a single lumped agonist and bulk aggregation, was introduced in Fogelson [Fogelson (1992)]. The aforementioned model was later extended in Fogelson [Fogelson (1993)] by introducing the capability to model multiple platelet agonists [Sorensen, Burgreen, Wagner et al. (1999a); Sorensen, Burgreen, Wagner et al. (1999b)]. Immersed-boundary-type models were reported in Fogelson et al. [Fogelson and Guy (2008)] to demonstrate the effect of thrombus development on the flow and the influence of fluid forces on thrombus growth. A study presented in Xu et al. [Xu, Chen, Kamocka et al. (2008)] sets out to explain blood flow influenced platelet aggregation and the size/geometry of the thrombus using a two-dimensional multi-scale model. Moreover, Merten et al. [Merten, Chow, Hellums et al. (2000)] used a Lagrangian description to investigate how platelets are activated. A numerical study based on combining the discrete element method (DEM) and the Stokesian dynamics method (SDM) was presented by Miyazaki et al. [Miyazaki and Yamaguchi (2002)] to analyse the mechanism of platelet adhesion. In addition, a number of other computational procedures were also adopted in the past [Ouareda, Choparda, Stahla et al. (2008); Rayz, Boussel, Ge et al. (2010); Peach, Ngoepe, Spranger et al. (2014); Ou, Huang and Yuen (2017); Yazdani, Li, Humphrey et al. (2017); Bouchnita and Volper (2019); Ye, Shi, Phan-Thien et al. (2019); Yesudasan and Averett (2019)].

Recently, a new class of Lagrangian technique called particle-based methods were developed to investigate the behaviour of corpuscles and their interactions in blood flow [Boryczko, Dzwinel and Yuen (2003); Filipovic, Kojic and Tsuda (2008)]. A mechanical model is proposed in Filipovic et al. [Filipovic, Kojic and Tsuda (2008)] that uses the dissipative particle dynamics (DPD) method to demonstrate the accumulation of platelets and their behaviour in blood flow.

Meanwhile Kamada et al. [Kamada, Tsubota, Nakamura et al. (2010)] used a particle-based technique described as moving particle semi-implicit (MPS) method to simulate the formation of thrombogenesis in both 2- and 3-dimensionsional scenarios. These methods highlighted the potential of particle-based methods in simulating thrombus formation and its interaction with blood flow.

This paper focuses on using a meshless particle based Lagrangian numerical technique, the smoothed particles hydrodynamics (SPH) method, to study the flow behaviour of blood and to explore the flow conditions that induce the formation of thrombus in a blood vessel. The particle nature of SPH method facilitates a convenient platform to model platelets which are in theory characterised as discrete particles. Further, this particle representation implies that the Lagrangian flow models can be easily and efficiently implemented with SPH technique. Thus, due to its simplicity and effectiveness, the SPH method is employed here to simulate the process of thrombogenesis under the influence

of various blood flow parameters. In the present SPH simulation, blood is modelled by two sets of particles which have the characteristics of plasma and of platelets, respectively. Flow simulations were conducted under flow conditions with different Reynolds numbers. The results obtained from simulations are compared with experimental results to validate the accuracy of the proposed methodology.

To validate the accuracy of the computational model proposed in this paper, two benchmark cases namely Poiseuille flow and downstream-facing step flow are initially tested and results are compared with the analytical solutions. Following these initial verifications of the computational model, numerical simulations of blood flow models are tested and compared with experimental data available in the literature.

2 Numerical methodology

Let ρ, t, v, $\mathbf{v}$ and p represent the fluid parameters density, time, kinematic viscosity, velocity and pressure of the fluid particles and $\mathbf{F}$ represents the external force acting on the fluid particles, then, the governing mass and momentum conservation equations for solving isothermal fluid flow using SPH are given by:

$$\frac{1}{\rho}\frac{D\rho}{Dt} + \nabla.\mathbf{v} = 0 \tag{1}$$

$$\frac{D\mathbf{v}}{Dt} = -\frac{1}{\rho}\nabla P + v\nabla^2.\mathbf{v} + \mathbf{F} \tag{2}$$

The velocity of each particle is updated from time step *n* to time step *n+1*, with the time step size of Δt, from the momentum equation Eq. (2) as:

$$\mathbf{v}^{n+1} = \mathbf{v}^n + \left(-\frac{1}{\rho}\nabla P^n + v\nabla^2.\mathbf{v}^n + \mathbf{F}^n\right)\Delta t \tag{3}$$

The position and density of the fluid is updated at each time step by

$$\mathbf{x}^{n+1} = \mathbf{x}^n + \mathbf{v}^{n+1}\Delta t \tag{4}$$

and (from the continuity equation Eq. (1)),

$$\rho^{n+1} = \rho^n - \rho^n(\nabla.\mathbf{v}^{n+1})\Delta t. \tag{5}$$

The pressure is estimated from the updated density using the equation of state [Batchelor (1967)]. The time step (Δt) is selected based on appropriate stability conditions for the given problem. For the numerical simulation considered in this paper, the time step is defined [Bonet and Lok (1999)] as a function of the Courant-Friedrichs-Lewy (C_{FL}) number ($0 < C_{FL} \leq 1$) and the speed of sound $c = \sqrt{\gamma k/\rho}$.

$$\Delta t = C_{FL}\frac{h}{\max(c + \|\mathbf{v}\|)} \tag{6}$$

Here γ, k are dimensionless constant and bulk modulus respectively. In the numerical simulations the incompressibility of the fluid is enforced by an artificial bulk modulus k [Monaghan (1994)] defined by:

$$k = {c_{max}^2 \rho}/{\gamma} \; ; \; c_{max} = m \, \|\mathbf{v}\|_{max} \tag{7}$$

The values of m in Eq. (7) are chosen between 10 and 1000 to impose fluid incompressibility.

3 The SPH methodology

The SPH approximation of an arbitrary function $\boldsymbol{\phi}$ at a point $\mathbf{x}$ with N neighbouring particles $\mathbf{x}_{\boldsymbol{b}}$ with volumes $\boldsymbol{V_b}$, kernel function $\boldsymbol{W_b}(\mathbf{x})$ and nodal variable $\boldsymbol{\phi_b}$ can be written in a discrete form as Bonet et al. [Bonet and Kulasegaram (2000a); Bonet and Kulasegaram (2000b, 2002)]:

$$\phi(\mathbf{x}) = \sum_{b=1}^{N} V_b \phi_b W_b(\mathbf{x}) \; ; \quad W_b(\mathbf{x}) = W(\mathbf{x} - \mathbf{x}_b, h) \tag{8}$$

The volume of particle $\mathbf{x}_b$ is the ratio of its mass m_b to its density ρ_b:

$$V_b = \frac{m_b}{\rho_b} \tag{9}$$

There are a number of different kernel/weight functions used in the SPH literature. The kernel function chosen here is a higher order quintic spline kernel function:

$$W(\mathbf{x} - \mathbf{x}', h) = \frac{\alpha}{h^d} \begin{cases} (2-q)^5 - 16(1-q)^5 & q \le 1 \\ (2-q)^5 & 1 < q \le 2 \\ 0 & q > 2 \end{cases} \; ; q = \frac{\|\mathbf{x} - \mathbf{x}'\|}{h} \tag{10}$$

where d is the number of dimensions of the problem and α is a scaling factor, $\mathbf{x}'$ is a sample position, h is the length parameter, which has a similar interpretation to element size in finite elements. The gradient of any arbitrary function ϕ can be evaluated from Eq. (8) as:

$$\nabla\phi(\mathbf{x}) = \sum_{b=1}^{N} V_b \, \phi_b \nabla W_b \tag{11}$$

The application of Eq. (8) to calculate the approximate value of the density of a continuum leads to the classical SPH equation given by:

$$\rho(\mathbf{x}) = \sum_{b=1}^{N} m_b W_b(\mathbf{x}). \tag{12}$$

Following from Eq. (11), the approximation of the gradient of the pressure in the momentum equations is:

$$(\nabla P)_a = \sum_{b=1}^{N} V_b P_b \nabla W_b(\mathbf{x}) \tag{13}$$

where b is the neighbouring particle within the support domain. Adopting the SPH approximations defined above, the divergence of the velocity field writes,

$$(\nabla . \mathbf{v}) = \sum_{b=1}^{N} V_b \mathbf{v}_b \, . \nabla W_b(\mathbf{x}) \tag{14}$$

In the above equations, the kernel function and its gradient must be corrected to achieve linear consistency. In this work kernel and gradient corrections are implemented as detailed in Bonet et al. [Bonet and Kulasegaram (2000a, 2000b, 2002)].

4 Boundary conditions

Due to the truncation of kernel functions at and near domain boundaries, the accuracy of SPH interpolation or approximation will be affected. In SPH formalism, the boundary conditions can be enforced through various numerical procedures: the repulsive force method [Monaghan (1994)], mirror particles method [Cummins and Rudman (1999); Takeda, Miyama and Sekiya (1994)], dummy particles-based method [Amini, Emdad and Farid (2011); Lee, Moulinec, Xu et al. (2008); Robert, Dalrymple and Knio (2000); Shao and Lo (2003)] and many others. Due to its simplicity and effectiveness the dummy particles method is adopted here to impose the wall boundary conditions.

In dummy particles method, usually four rows of dummy particles are placed outside the boundary [Shao and Lo (2003)] as shown in Fig. 2. The distance between the rows of dummy particles depends on the kernel smoothing length h (which is usually half of kernel base radius). If the smoothing length h=2$\hat{r}$, where $\hat{r}$ denotes the initial particle spacing, four lines of dummy particles at a spacing of $\hat{r}$ between the lines to be used to enforce the boundary conditions. This is to ensure that the SPH approximation can be performed without any loss of accuracy arising from truncation of the kernel function. The velocity of these dummy particles is set to zero, which enforces non-slip Dirichlet (**v**=0) boundary conditions at the wall boundaries. The pressure on the particles at edges and normal to the wall surface are identical to the pressure at the fixed dummy particles. This procedure will enforce Neumann ($\frac{\partial P}{\partial n} = 0,\ n - boundary\, normal$) pressure boundary conditions at the wall boundaries and these boundary conditions can be easily introduced in the governing fluid flow equations [Cummins and Rudman (1999)]. In addition, irregular or complex boundary contours can also be handled in a similar procedure as demonstrated by Lee et al. [Lee, Moulinec, Xu et al. (2008)].

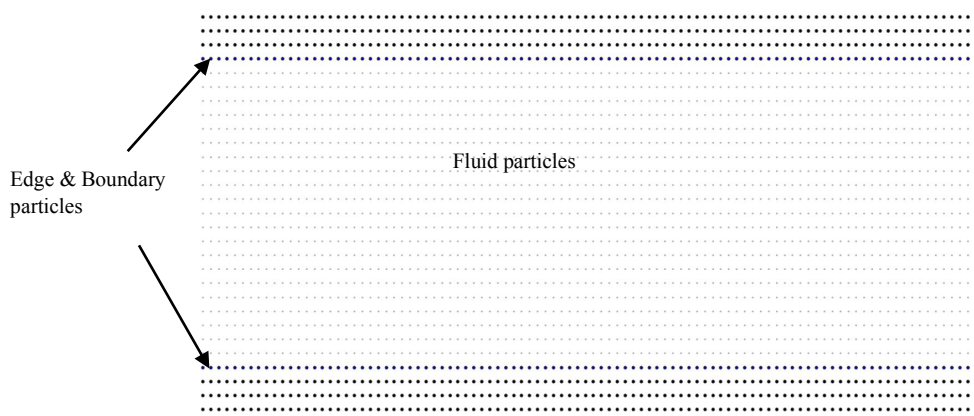

Figure 2: SPH discretisation of fluid with boundary dummy particles

5 Numerical verification of the computational model

Prior to investigating the application of SPH methodology described above for blood flow simulations, it is useful to examine the ability and accuracy of the SPH method in simulating related standard benchmark fluid flow problems. Two such cases are

considered here to verify our SPH code. These are the Poiseuille flow and the downstream-facing step flow. Tab. 1 illustrates the geometries and boundary conditions of the numerical examples considered in this section.

Table 1: Test cases and model parameters

No.	Test case	Domain dimension & Flow characteristics
1.	Poiseuille flow	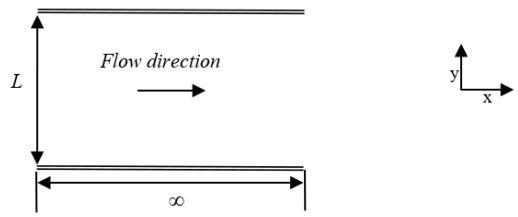
2.	Downstream-facing step flow	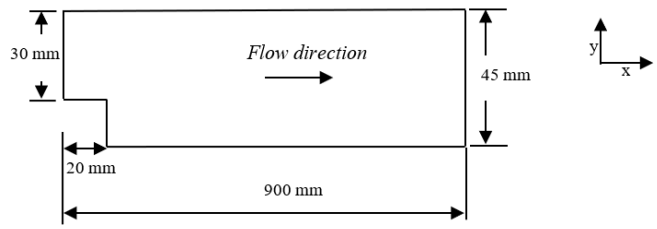

5.1 Poiseuille flow

The first numerical test considered in this section is the Poiseuille flow, which consists of flow between two parallel infinite plates. The fluid is driven by an axial pressure difference thus enforcing the flow to be parallel to the infinite plates. The fluid is accelerated due to a directional pressure difference which can be interpreted as an external body force, as described by the momentum equation Eq. (3). In this example, the plates are located at $y = 0$ and $y = L$ as illustrated in Tab. 1. The fluid is accelerated from rest until it reaches a steady state. The numerical results (i.e., velocity with respect to time) are compared with analytical solutions in Morris et al. [Morris, Fox and Zhu (1997)]. The density and dynamic viscosity used in the numerical simulations are $1000\,\mathrm{kg/m^3}$ and $1 \times 10^{-6}\ \mathrm{m^2/s}$ respectively. In addition, the simulations were also performed for two different geometrical cases, with the distance L between the plates 0.005 m and 0.0025 m, to investigate the flow with two different Reynolds numbers ($Re = \frac{UL}{v}$) . A uniform spacing between particle (i.e., $\Delta x = \Delta y = 0.0001$ m and 0.00005 m) corresponding to 50 particles in the span between the plates were used in the case of both Reynolds numbers. The results of the simulation are shown in Fig. 3 and are compared with the analytical solution. It can be noted that the numerical results are in close agreement with the analytical solution.

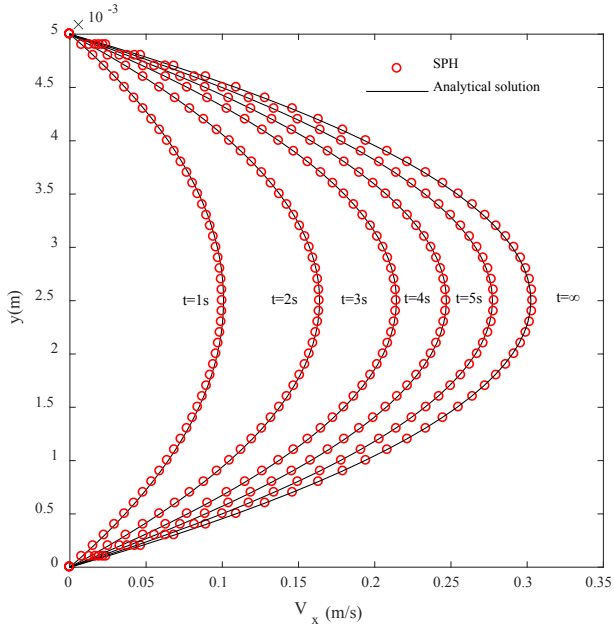

(a)

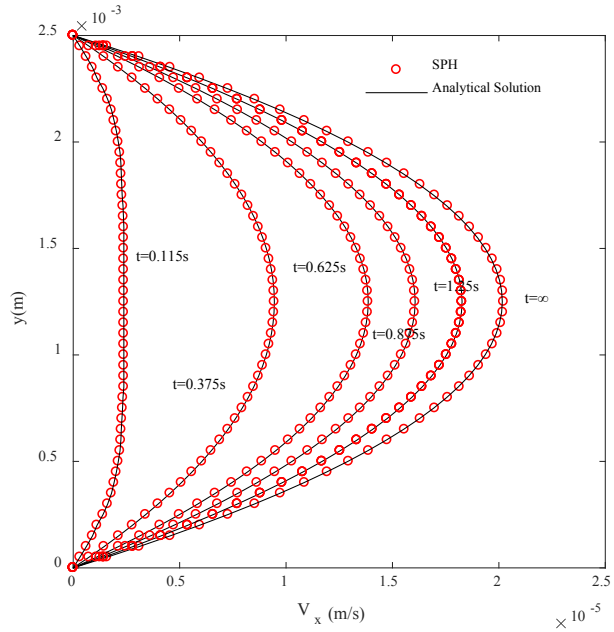

(b)

Figure 3: Development of velocity profiles of the Poiseuille flow for (a) *Re*=1500 and (b) *Re*=0.05

We now investigate the influence of the spatial resolution of fluid particles on numerical results. The results are shown in Fig. 4, which indicates the effect of particle resolution on the accuracy of the numerical results obtained.

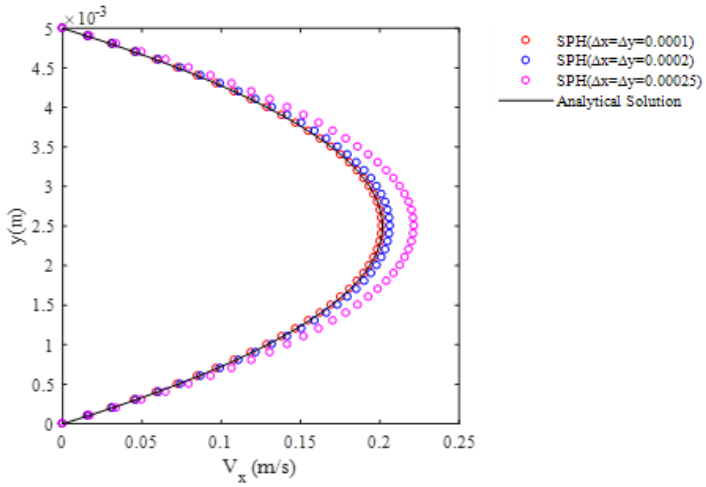

Figure 4: Velocity profiles for poiseuille flow at different resolutions with *R*e=1500 at t=3 s

The difference between the numerical simulation results and the analytical solution is determined using the Relative error equation, which is defined as,

$$\text{Relative error} = \sqrt{\frac{\sum_{i=1}^{N}\left(A_{i,SPH}-A_{i,Exact}\right)^2}{\sum_{i=1}^{N}\left(A_{i,Exact}\right)^2}} \tag{15}$$

where $A_{i,SPH}, A_{i,Exact}$, are the SPH and exact analytical solution for a chosen parameter *A* at particle 'i' and *N* is the total number of particles used to calculate the relative error. The results are compared with the analytical solution. The numerical results are in close agreement with the analytical solution. For the results illustrated in Figs. 3(a) and 3(b), the average relative error over all the particles in the domain at steady state, for Re=1500 and Re=0.05, is between 0.11%-0.48%. In the case of Re=1500 at t=3 s (Fig. 4), the maximum relative error is 0.42% for the peak velocity during the simulation and the average relative error over all the particles in the domain at steady state is 0.40%.

5.2 Downstream facing step flow

This is an important benchmark example as it contains a sudden change of cross-sectional area at the step, in combination with channel flow characteristics away from the step. Therefore, successful simulation of this benchmark can further establish the accuracy and applicability of the developed methodology for simulating blood flow in arteries. In this numerical simulation, a constant body force is applied to drive the flow at the entrance of the channel, where the body force is set to obtain a mean bulk velocity in the channel above the step (see Tab. 1.) with two different Reynolds numbers (i.e., Re=73 and Re=229). The density and dynamic viscosity of the numerical simulations are chosen as $1000\,\mathrm{kg/m^3}$ and $1 \times 10^{-6}\ \mathrm{m^2/s}$ respectively. Initially the fluid is discretised with

uniform spacing between particles (i. e., $\Delta x = \Delta y$). The velocity profiles at two different downstream locations are depicted in Figs. 5 and 6. It can be noted from these figures that the numerical results compare well with and converge to the experimental results in the literature [Denham (1974)].

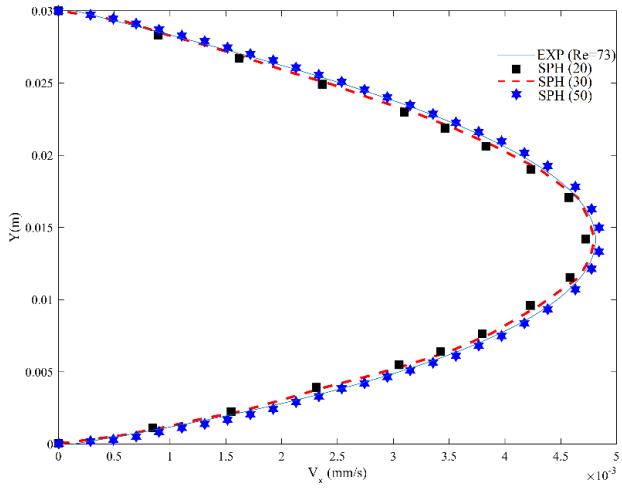

Position (Y)	% difference in velocities		
	SPH(20)	SPH(30)	SPH(50)
0.015	2.45	0.80	0.028
0.01	1.84	1.73	0.014
0.005	2.53	0.64	0.020
0.02	1.86	1.59	0.014
0.025	3.29	3.818	0.026

(a)

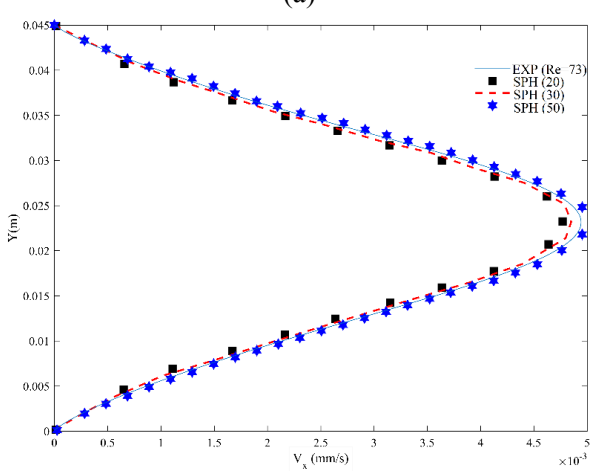

Position (Y)	% difference in velocities		
	SPH(20)	SPH(30)	SPH(50)
0.005	18.58	7.104	1.64
0.015	2.96	2.19	0.24
0.0225	3.28	1.62	0.46
0.03	2.48	2.15	0.66
0.04	18.07	12.62	3.43

(b)

Figure 5: Comparsion of the velocity profiles at (a) x=0 and (b) x=900 for Re=73

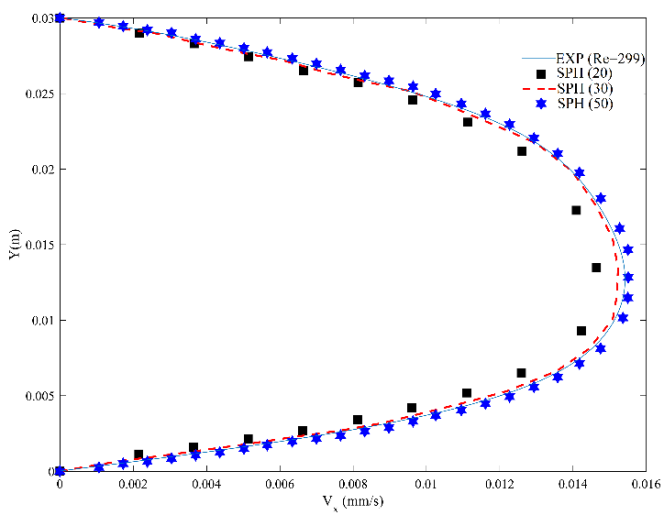

Position (Y)	% difference in velocities		
	SPH(20)	SPH(30)	SPH(50)
0.015	3.84	1.80	0.92
0.01	6.71	1.05	0.74
0.005	8.98	6.05	0.006
0.02	9.55	1.62	0.21
0.025	0.89	0.83	0.008

(a)

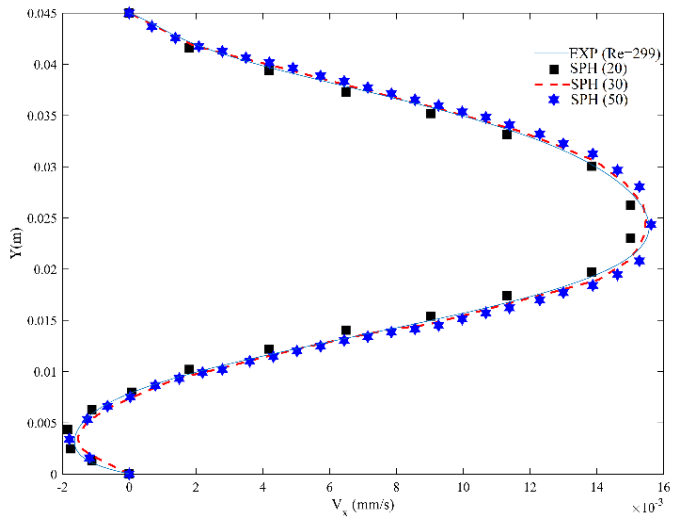

Position (Y)	% difference in velocities		
	SPH(20)	SPH(30)	SPH(50)
0.005	26.79	26.49	19.74
0.015	11.50	1.04	0.01
0.0225	1.29	1.16	0.43
0.03	0.65	0.35	0.13
0.04	40.44	15.43	0.05

(b)

Figure 6: Comparsion of the velocity profiles at (a) x=0 and (b) x=900 for Re=229

The numerical simulations of both benchmark test cases presented above clearly demonstrate the capability of the computational model developed. In addition, the effect of particle resolutions on the accuracy of the results is promising.

6 Modelling of blood flow

This section focuses on the application of the developed SPH methodology to model blood flow. Firstly, blood flow through a bifurcation artery is considered. This simulation is performed here to explore the accuracy of the proposed SPH method in modelling blood flow through arteries. A realistic blood vessel geometry of an artery bifurcation is chosen in the following section to perform numerical studies.

6.1 Blood flow through an artery bifurcation

The fundamental geometry of the bifurcating artery, which is identical to the model described in Gijsen et al. [Gijsen, Van de Vosse and Janssen (1999)] is illustrated in Fig. 7. The geometry of bifurcation artery consists of three main regions namely, common

carotid, internal carotid, and external carotid. The axial flow through cross-sections denoted by A, B, C and D is investigated in this numerical simulation. Cross-section A is located in the middle of the common carotid artery. Meanwhile, cross-sections B, C and D are located at different positions (in x'-axis) along the internal carotid as shown in Fig. 7. To study the accuracy of the numerical scheme, simulations were performed by discretising the fluid using different particle resolutions. The number of particles used to discretise the flow domain is 1000, 2000 and 5000 which are denoted here by SPH(1000), SPH(2000) and SPH(5000) respectively. The fluid is accelerated by a pulsatile pressure variation to mimic realistic blood flow. The Reynolds number of the flow simulation is 270. The viscosity and density of the fluid are assumed to be $2 \times 10^{-6}\ \mathrm{m}^2/\mathrm{s}$ and $1410\ \mathrm{kg}/\mathrm{m}^3$ respectively. The diameter of the common carotid was chosen as 6.2 mm. The velocity profiles across sections A, B, C and D are illustrated in Fig. 8. It is evident from the figure that the numerical results compare well with the experimental observations reported in literature [Gijsen, Van de Vosse and Janssen (1999)].

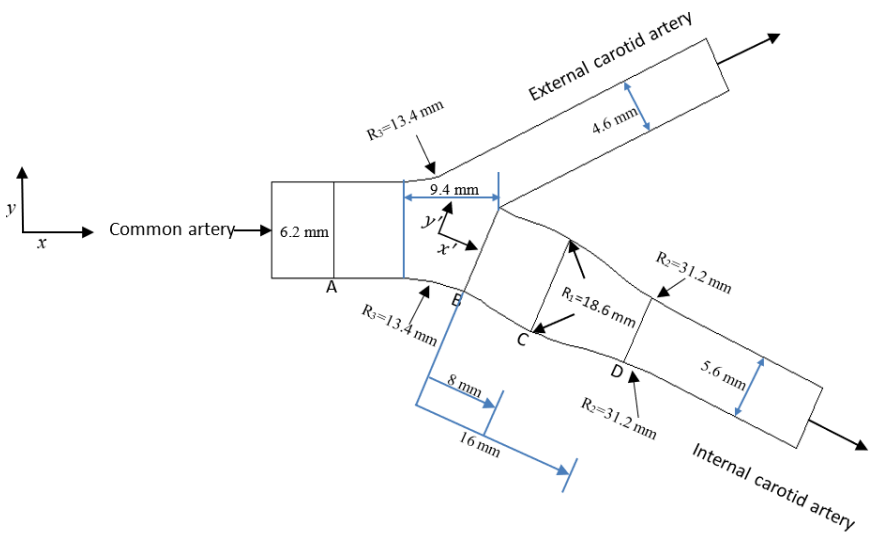

Figure 7: The configuration geometry of bifurcation artery

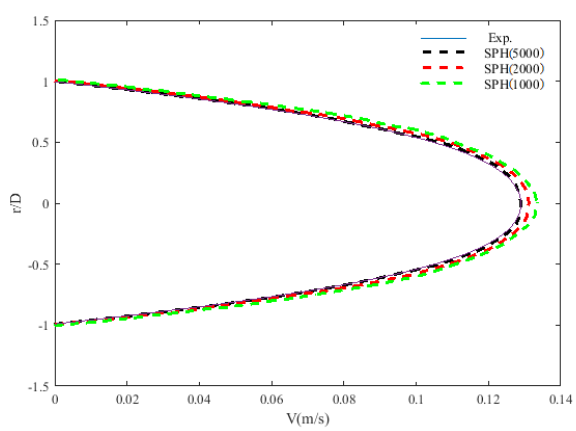

Position (r/D)	% difference in velocities		
	SPH (1000)	SPH (2000)	SPH (5000)
0.4	0.29	0.29	0.19
0.2	2.73	1.67	0.35
0	3.84	2.09	0.34
-0.2	2.73	1.67	0.35
-0.4	0.29	0.29	0.19

(a)

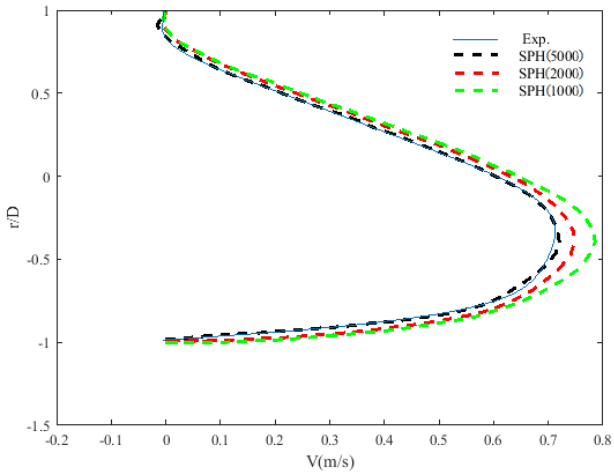

Position (r/D)	% difference in velocities		
	SPH (1000)	SPH (2000)	SPH (5000)
0.4	1.63	1.63	0.00049
0.2	0.82	6.99	0.00031
0	2.65	2.65	016
-0.2	6.70	2.93	0.27
-0.4	9.27	4.03	0.13

(b)

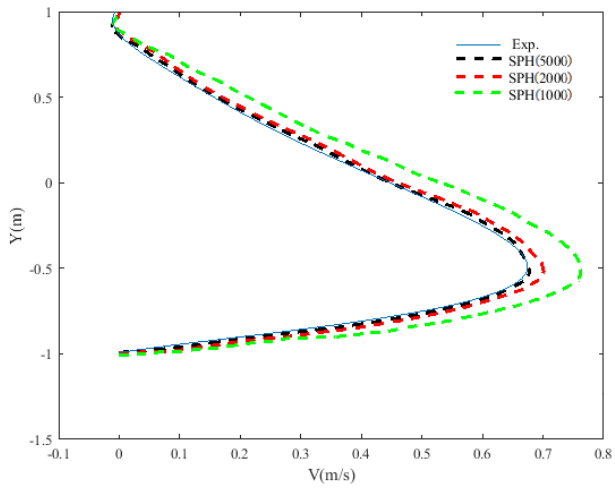

Position (r/D)	% difference in velocities		
	SPH (1000)	SPH (2000)	SPH (5000)
0.4	25.34	8.28	3.82
0.2	17.58	4.78	2.58
0	15.61	3.85	1.65
-0.2	12.95	2.93	1.04
-0.4	13.92	3.64	0.95

(c)

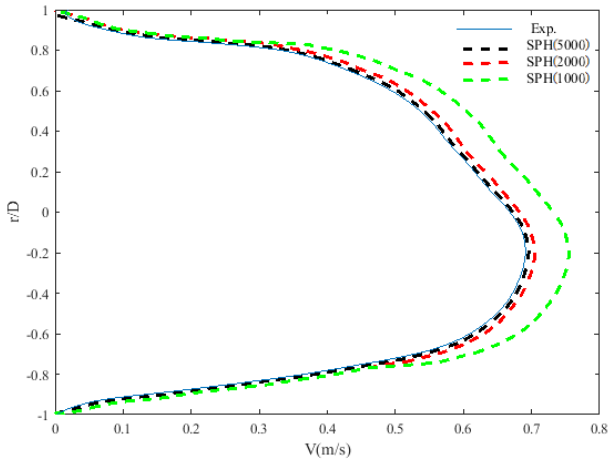

Position (r/D)	% difference in velocities		
	SPH (1000)	SPH (2000)	SPH (5000)
0.4	11.95	4.58	0.84
0.2	10.70	3.75	0.62
0	9.70	3.86	0.59
-0.2	9.34	4.22	0.70
-0.4	9.63	4.06	0.87

(d)

Figure 8: The comparison of results for the velocity profiles at cross-sections A (a), B (b), C (c) and D (d)

6.2 Modelling platelet motion and thrombus formation

The purpose of this study is to simulate formation of a thrombus and to investigate the applicability of SPH in modelling similar physiological processes. The corrected SPH method is used in the modelling to improve the accuracy [Bonet and Kulasegaram (2000a, b)] of the simulation.

Platelets tend to adhere and aggregate when a blood vessel is damaged. This can lead to the formation of primary thrombus. Inside the primary thrombus, the platelets link together, and are then bonded by fibrinogen in plasma and collagen in the sub-endothelial tissue [Savage, Saldívar and Ruggeri (1996)]. To numerically model platelet motion, an algorithm based on a penalty or spring force mechanism [Kamada, Tsubota, Nakamura et al. (2010)] is adopted. This model simulates the interactions between platelets and plasma inside the blood vessel. When the platelets are within a distance d_{ad} from the damaged area, the platelets adhere to the wall by an adhesive force as given by Eq. (16). The platelets adhered to the wall are activated and attract other platelets which are within a distance of d_{ag} from them as illustrated in Fig. 9. This attractive force is called an aggregation force and is defined by Eq. (17). This aggregation force is algebraically similar to that of the adhesive force on the platelets but has a different spring constant compared to the adhesive force.

$$F_{ad} = \begin{cases} K_{ad}(|\boldsymbol{r}_{ij}| - r_o)\boldsymbol{n}_{ij} & (|\boldsymbol{r}_{ij}| \le d_{ad}) \\ 0 & (|\boldsymbol{r}_{ij}| > d_{ad}) \end{cases} \tag{16}$$

$$F_{ag} = \begin{cases} K_{ag}(|\boldsymbol{r}_{ij}| - r_o)\boldsymbol{n}_{ij} & (|\boldsymbol{r}_{ij}| \le d_{ag}) \\ 0 & (|\boldsymbol{r}_{ij}| > d_{ag}) \end{cases} \tag{17}$$

In the above equations $\boldsymbol{F}_{ad}, \boldsymbol{F}_{ag}$ are the adhesive and aggregate forces respectively and K_{ad}, K_{ag} are the corresponding spring constants. The $\boldsymbol{r}_{ij}$ here is the distance between

activated platelets and the vessel wall (or other non-activated platelets), is the original or non-activated inter-particle distance and $\boldsymbol{n}_{ij}$ is a unit vector linking platelet and damaged wall (or linking activated platelet and other surrounding platelets). During the numerical simulations, the forces defined above are introduced in Eq. (2) as external forces acting on platelet particles which are within the region of influence by adhesion and aggregation.

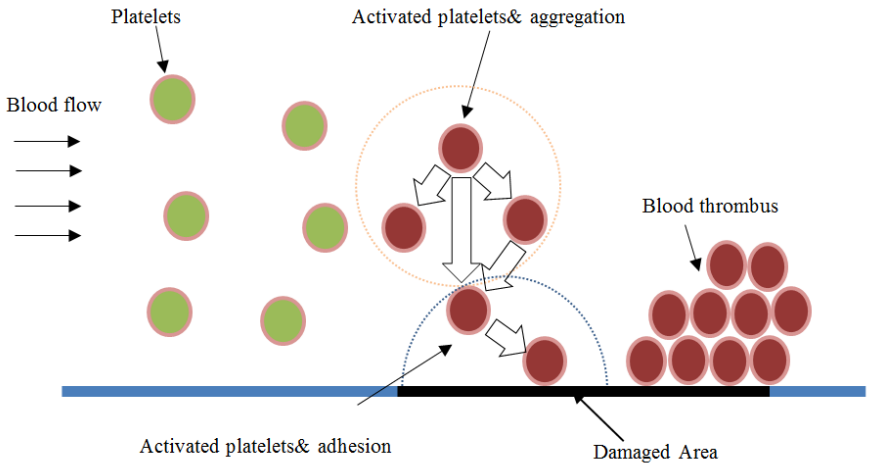

Figure 9: Method of platelet adhesion and aggregation at a damaged area of a vessel

7 Numerical experiments

7.1 Blood flow through straight vessel

First, the blood flow simulations were performed inside a straight blood vessel with different flow velocities between 100 and 700 μm/s, which were defined at the inlet of the blood vessel. The total length of the vessel (L) and the width between the two walls (D) are, respectively, 130 μm and 40 μm. The length of the damaged wall (L_i) is 40 μm and the distance from the inlet to the damaged wall (L_o) is 40 μm (see Fig. 10(a)). The total number of particles used in the simulation was 5371. Four layers of boundary dummy particles were also used. For clarity and for better visualisation, the plasma (red background) and the platelets (dark points) are represented as illustrated in Fig. 10(b). The initial distance between particles is 1.0 μm. The density ρ and kinematic viscosity v of the plasma and platelets were set as $1\text{x}10^3$ kg/m^3 and $1\text{x}10^{-6}$ m^2/s respectively. The boundary conditions were a uniform velocity at the inlet, zero pressure at the outlet and non-slip condition at the walls enforced by dummy boundary particles. The amount of platelet particles used is approximately 9% of the plasma which is higher than normal physiological condition to reduce simulation time for thrombus formation. The time step of the simulation was set to $5\text{x}10^{-7}$ s to ensure the stability of numerical integration scheme. After performing systematic repetitive simulations to achieve numerical results that were consistent with reported experimental observations [Begent and Born (1970); Xu, Chen, Kamocka et al. (2008)], appropriate spring constant values were determined for adhesion and aggregation.

The determined spring constant values for K_{ad} and K_{ag} were $9.0\text{x}10^9$ N/m and $4.5\text{x}10^9$ N/m, respectively, while d_{ad}=2.0 μm=d_{ag}, and r_o=2.0 μm.

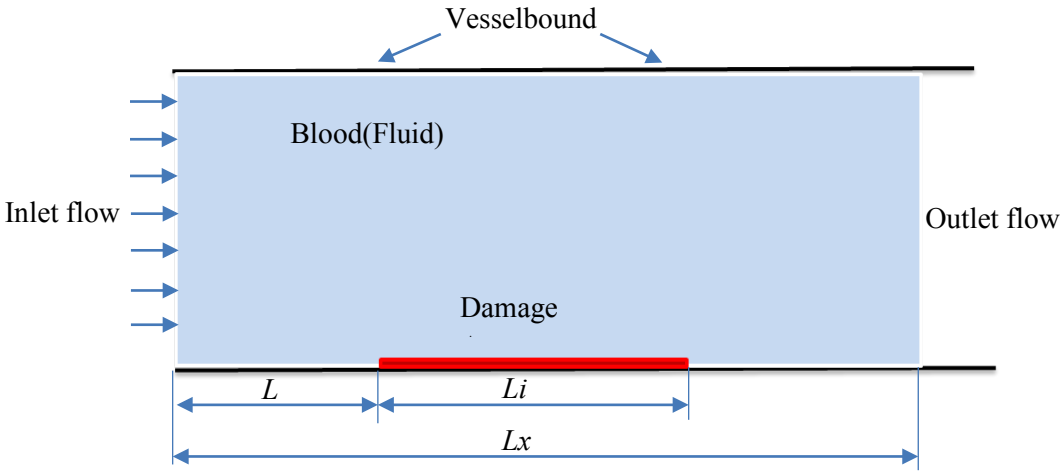

(a)

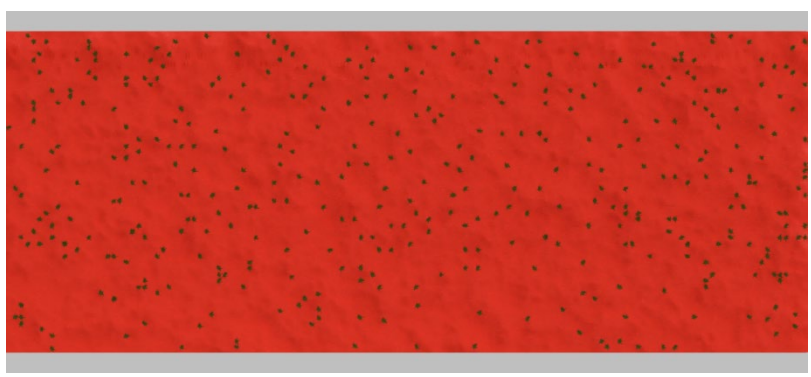

(b)

Figure 10: Schematic diagram of (a) a straight vessel and (b) arrangment of particles

Normally, a thrombus is formed by adhesion and aggregation of platelets, which are transported by the blood flow through different geometries of arteries or vessels. The growth rate of thrombus formation varies with the stenosis and the flow rate of blood. Fig. 11 illustrates the formation of a thrombus at various stages of the flow. The platelets are activated when they are within the d_{ad} distance from the damaged region and form a primary thrombus. During the course of time, a primary thrombus is developed to cover the whole damage area by forming several layers of platelets. When the thrombus grows to a certain volume, part of the thrombus is separated and transported downstream by the blood flow. Fig. 12 compares thrombus formation for two different particle resolutions. Figs. 13-15 depict the growth of the thrombus at different times for blood flow velocities 100, 500 and 700 μm/s respectively. From these figures, various stages of thrombus growth on the damaged area of the wall are evident. It can be noted from Figs. 13(b), 14(b) and 15(b) that part of the thrombus is separated from the primary thrombus once

the primary thrombus grows to a substantial volume. It is interesting to observe that the volume of the primary thrombus and the time at which separation of the thrombus takes place are influenced by the flow rate. From these figures, it can also be noted that when the flow rate is 700 μm/s the thrombus growth is thinner compared to the cases where the blood flow rate is 100 and 500 μm/s. Further, as expected, it was observed that with higher flow rates the separation of thrombus takes place quicker.

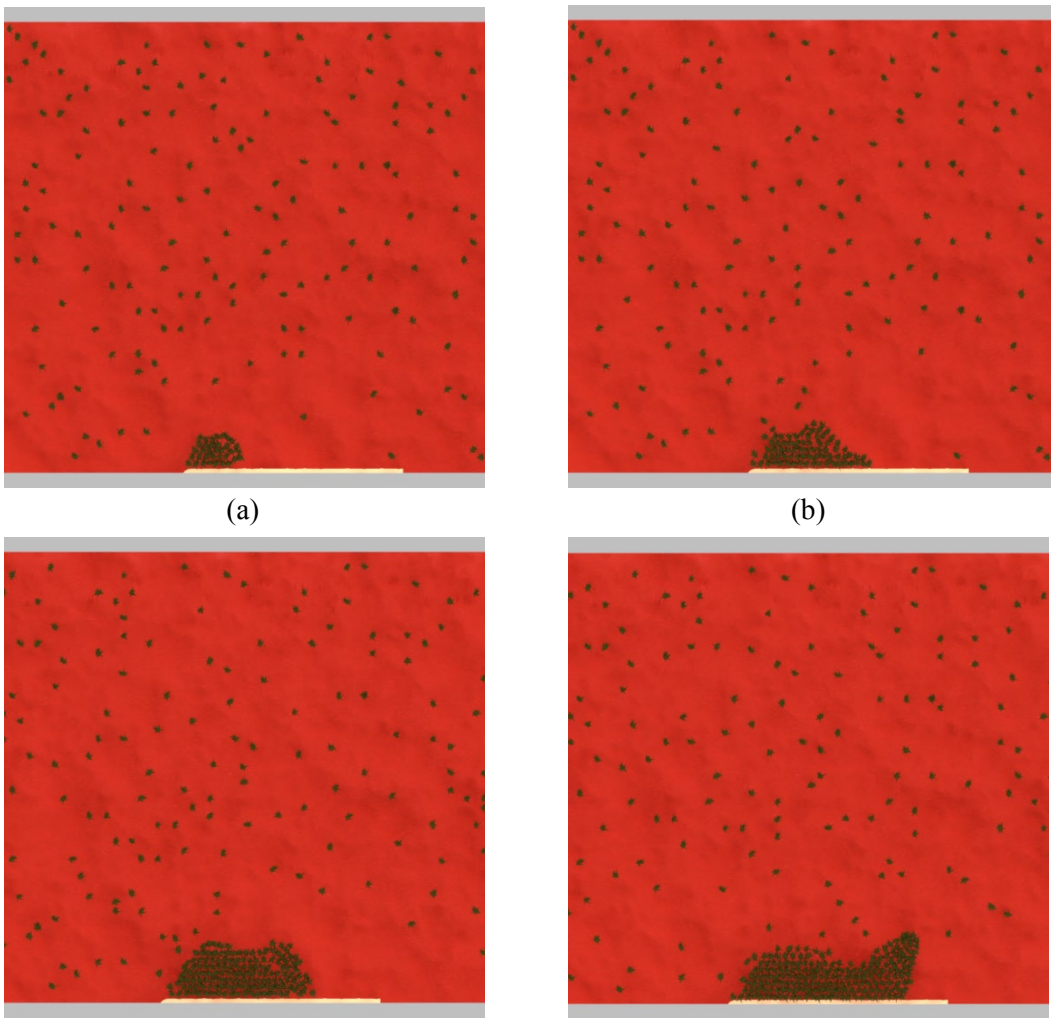

(a) (b) (c) (d)

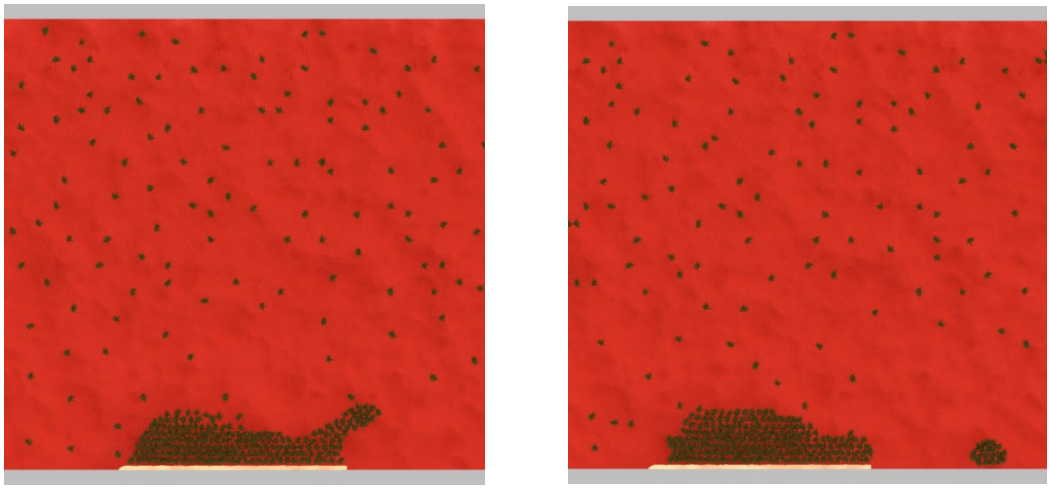

(e) (f)

Figure 11: Stages of thrombus formation and separation with time

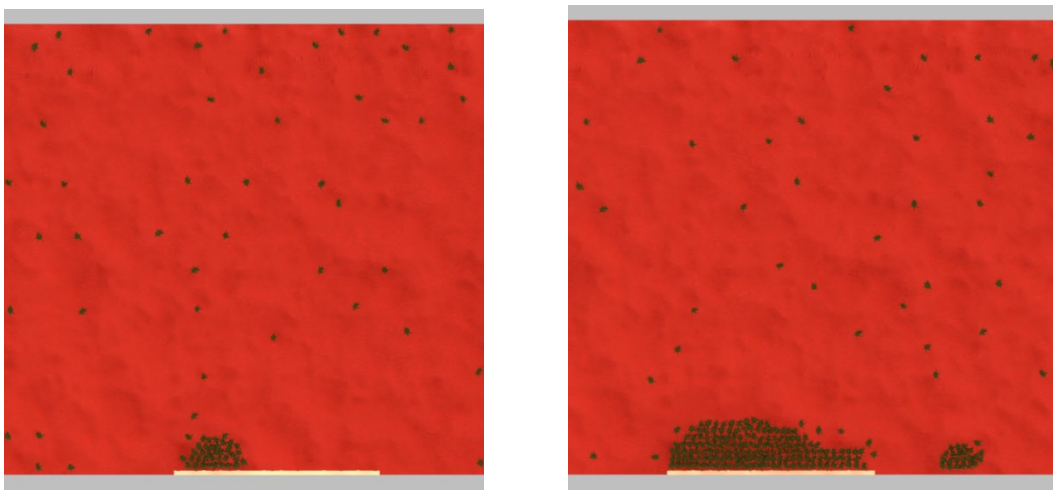

(a)

(b)

Figure 12: Comparison of different resolution of particles, for flow velocity 500 μm/s: (a) coarse particle distribution; (b) fine particles distribution

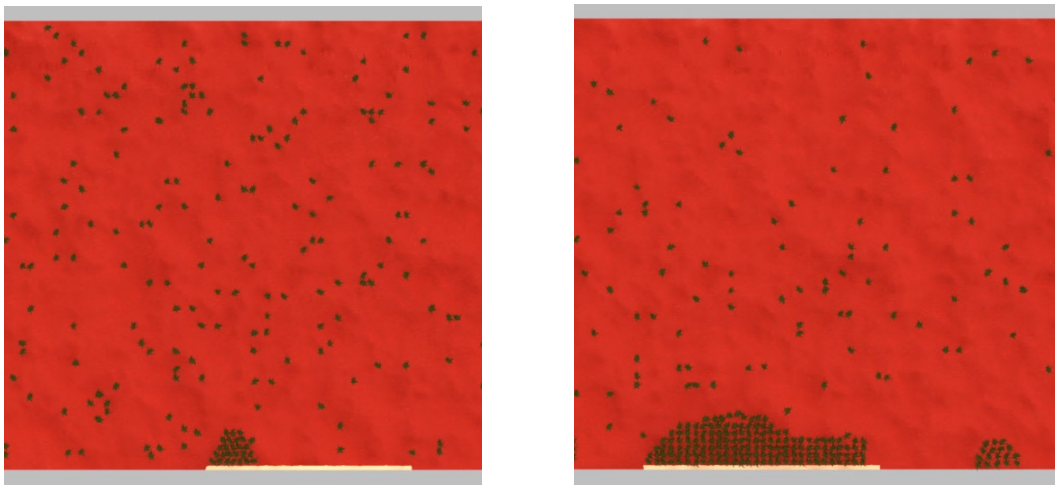

(a) (b)

Figure 13: The platelet aggregation for flow velocity 100 μm/s at (a) t=0.2 s (b) t=0.6 s

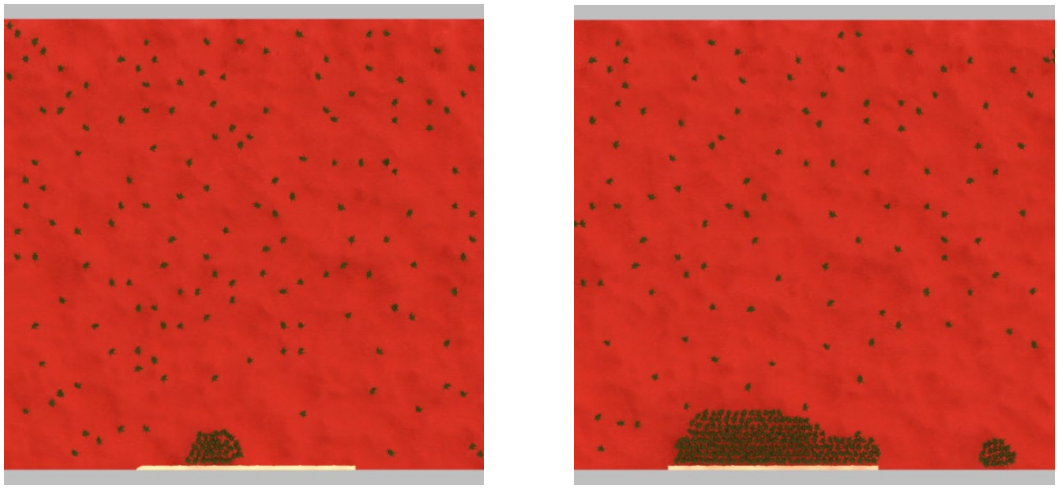

(a) (b)

Figure 14: The platelet aggregation for flow velocity 500 μm/s at (a) t=0.2 s (b) t=0.6 s

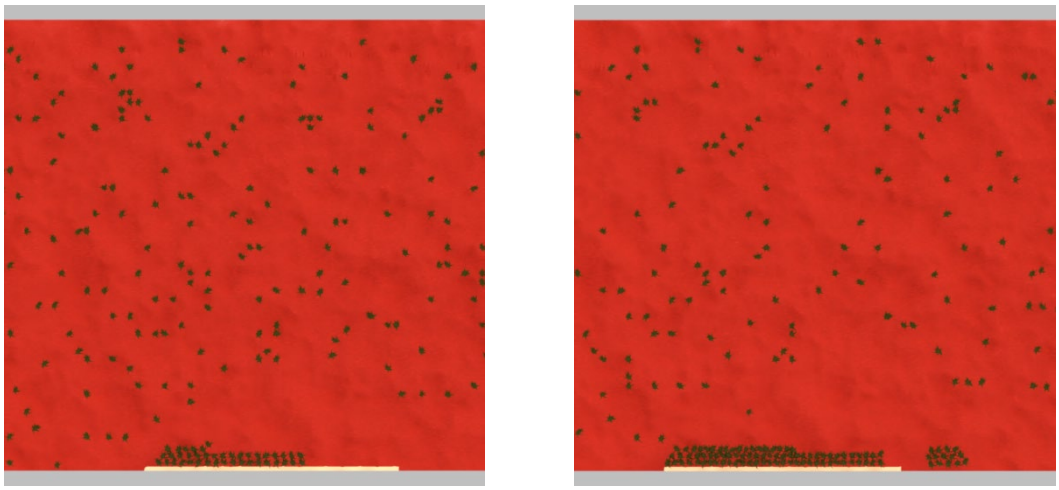

(a) (b)

Figure 15: The platelet aggregation for flow velocity 700 μm/s at (a) t=0.2 s (b) t=0.6 s

Fig. 16 plots the growth rate of thrombus against various blood flow velocities. It can be seen from Fig. 16 that the growth rate of the thrombus gradually increases with blood velocity until approximately 500 μm/s. Beyond 500 μm/s the thrombus growth rate drops to a lower level. The results illustrated in Fig. 16 qualitatively agree with the experimental observation made in Begent et al. [Begent and Born (1970)]. Given that the results reported here are from 2-dimensional simulations, direct comparisons cannot be made at this point. It is evident however that the blood flow rate plays a crucial role in the build-up and separation of a thrombus. The numerical results also indicate that the growth rate of the thrombus, its thickness, and formation/separation vary according to the blood flow rate and

these results are consistent with experimental observations reported in Begent et al. [Begent and Born (1970)]. To further establish the accuracy of the model developed in this article, a comparative study was conducted with a 2-dimensional simulation model reported in the literature [Xu, Chen, Kamocka et al. (2008)]. In this study, the number of platelets (size of the clots) adhered/aggregated at different blood flow rate was compared. Fig. 17 illustrates the comparative results obtained with our SPH model developed in this article and computational model reported by Xu et al. [Xu, Chen, Kamocka et al. (2008)]. It is evident from Fig. 18 that both simulation results compare well.

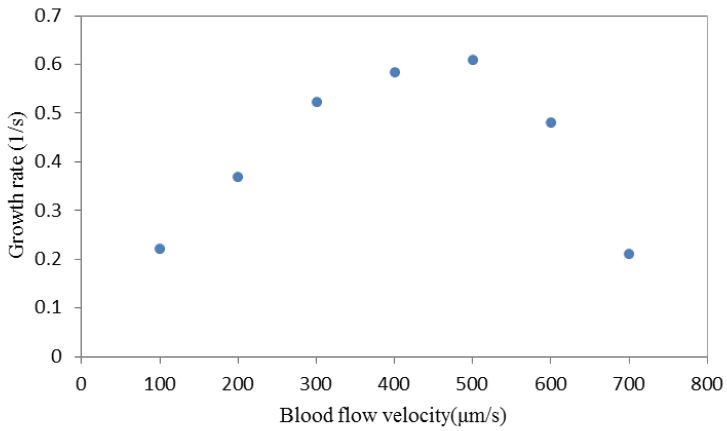

Figure 16: Effect of blood flow velocity on thrombus growth rate

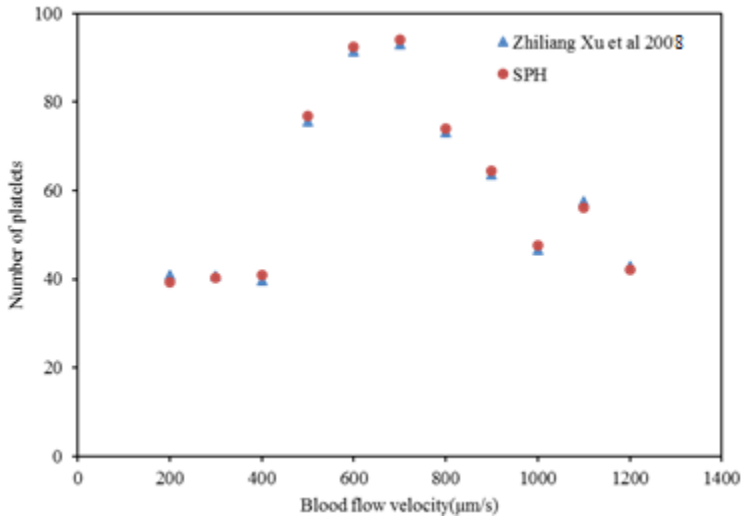

Figure 17: Effect of blood flow velocity on the number of platelets aggregated

7.2 Blood flow through vessels with bend

To investigate the effect of vessel geometry on thrombus formation and its growth, blood vessels with 90° and 180° bend were chosen next. Figs. 18(a) and 18(b) show the two-dimensional vessel configurations. The damaged area in both configurations is approximately 20 μm long. The boundary conditions and flow parameters used in the simulations were same as that of straight vessel.

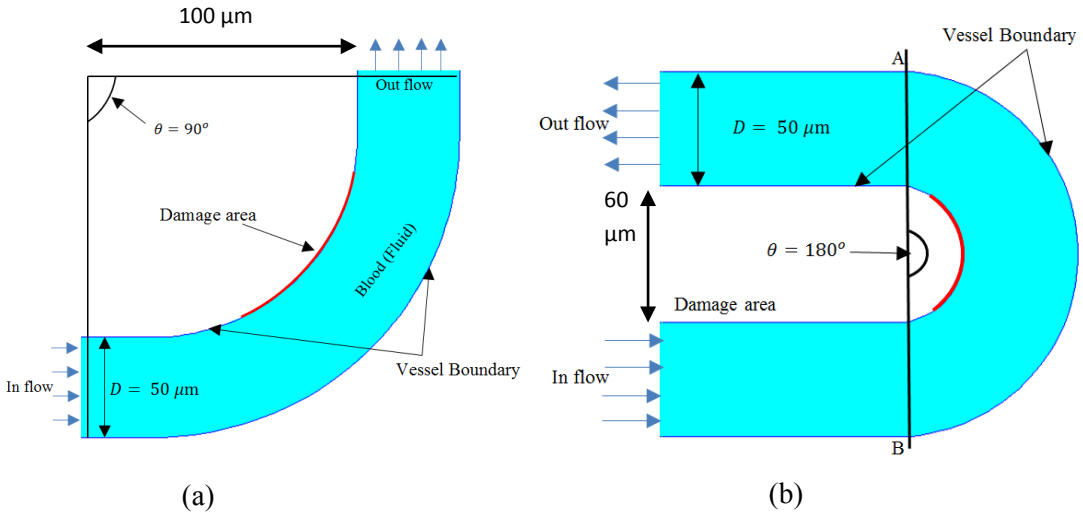

Figure 18: The geometry of vessels with (a) 90° and (b) 180° bends

Fig. 19 depicts the growth of a thrombus in a vessel that has 90° bend. The fluid velocity increases marginally towards the inner side of the bend where maximum velocity of the flow is reached. This causes less number of platelets to adhere and aggregate in the case of vessel with 90° bend at the same time (i.e., at 0.6 s), compare to straight vessel with the same damage area and fluid entry velocity. Fig. 19 also indicates that, after the thrombus developed into a substantial volume, it was destroyed by the blood flow and transported downstream of the vessel. Fig. 20 describes the growth of a thrombus in a vessel that has 180° bend. It can be noted that, the number of platelets adhere and aggregate on the damaged area of the vessel for 180° bend is different from those in the vessel with 90° bend. As the maximum velocity is towards the inner side of the bend, and the velocity for 180° bend will be larger than in the vessel with 90° bend, the number of platelets adhere and aggregate in the case of vessel with 180° bend is less. As a result, in Fig. 20(b) with fluid entry velocity 100 μm/s, the damaged area is covered with only a monolayer of platelets. As it can be noted from Fig. 21, with a higher fluid entry velocity 700 μm/s, the number of platelets adhere and aggregate are significantly less compare to that of entry velocity 100 μm/s and the characteristics of thrombus growth/transportation were entirely different to that of straight vessel and the vessel with 90° bend. From these numerical results, it is apparent that the growth and separation of thrombus are significantly influenced by the curvature of the vessel and the flow rate.

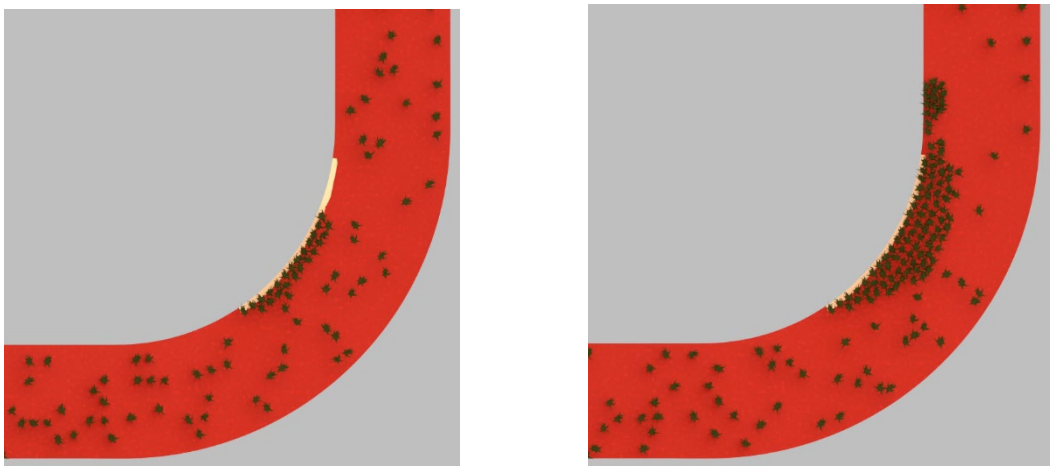

(a) (b)

Figure 19: The platelet aggregation for entry velocity 100 μm/s at (a) t=0.2 s (b) t=0.6 s

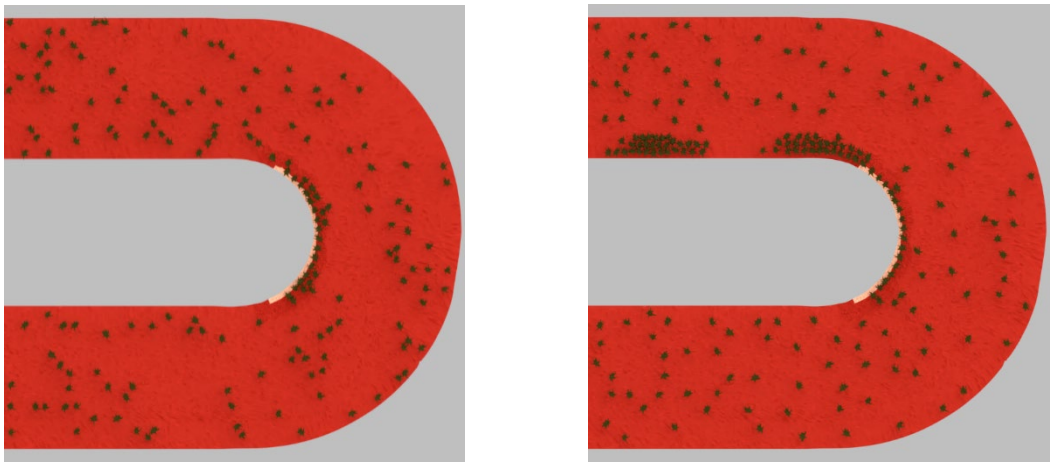

(a) (b)

Figure 20: The platelet aggregation for entry velocity 100 μm/s at (a) t=0.2 s (b) t=0.6 s

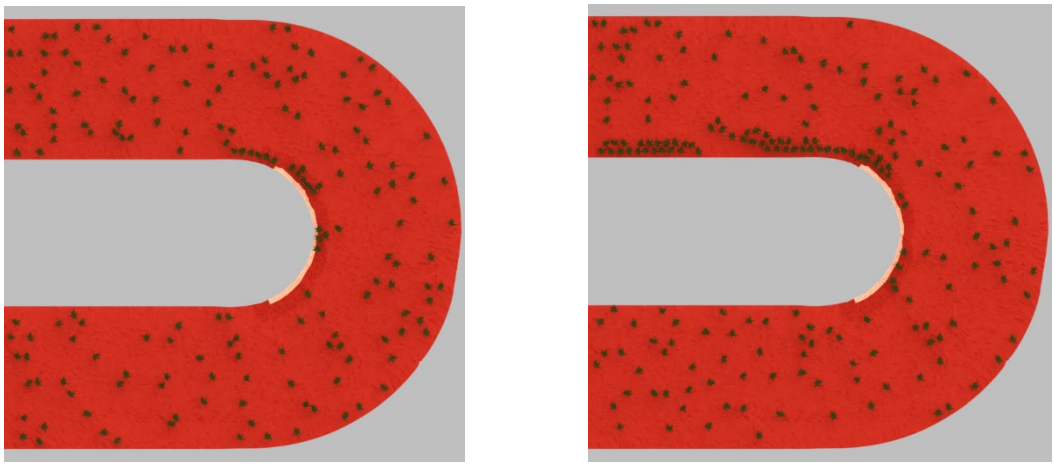

(a) (b)

Figure 21: The platelet aggregation for entry velocity=700 μm/s at (a) t=0.2 s (b) t=0.6 s

7.3 Blood flow through a stenosed vessel

In some diseases of the coronary artery, the vessel progressively narrows because of arterial plaque, called an atheroma, in the intimal layer. The atheroma consists of smooth muscle cells, lipids, collagen, elastin, and sometimes calcium deposits. The constriction caused by the atheroma is clinically referred to as a stenosis [Ku (1997)]. In order to analyse thrombus formation in a straight vessel with an internal and local geometric variation, the blood flow through a stenosed vessel is examined in this section. The aim in this simulation is to determine the modelling parameters that will reproduce qualitatively comparable results with respect to experimental observations reported in literature. Fig. 22 illustrates the initial geometry of the stenosed vessel which is based on the geometrical description provided in Bark [Bark (2007)]. The total length of the vessel is 300 μm and the stenosed area is in the middle of the vessel. The length of the damaged area is 16 μm. The diameter of the vessel is 75 μm. As per the geometry, the vessel contains 85% stenosis by cross-sectional area. The initial distance between particles is $(\Delta x = \Delta y =)1.0$ μm. The density ρ and kinematic viscosity v of the plasma and platelets are set as $1\text{x}10^3\ \text{kg/m}^3$ and $1\text{x}10^{-6}\ \text{m}^2/\text{s}$ respectively. The amount of the platelet particles used in this simulation is approximately 7% of the plasma. The entry velocity of the blood flow is 5 μm/s. The numerical simulations with various parametric values for the spring constants (K_{ad}, K_{ag}), the adhesion area (d_{ad}) and the aggregation area (d_{ag}) were repeated until a qualitative match was obtained between the numerical simulations and experimental results reported in literature. From the numerical tests, the best parametric values obtained for spring constants K_{ad} and K_{ag} were $9.0\text{x}10^9\ \text{N/m}$ and, $5.0\text{x}10^9\ \text{N/m}$ respectively. Further, the suitable parametric values for adhesion area (d_{ad}) and aggregation area (d_{ag}) were found to be 2.0 μm and 4.0 μm, respectively. It can be noted from these resulted parametric values that the aggregation area d_{ag} is doubled in this simulation compare to previous numerical examples to reproduce thrombus location and growth similar to that of experimental results [Flannery (2005)]. In

addition, the spring constant for aggregation K_{ag} is also slightly modified to adapt the shape of the thrombus to match the observation reported in the experiment.

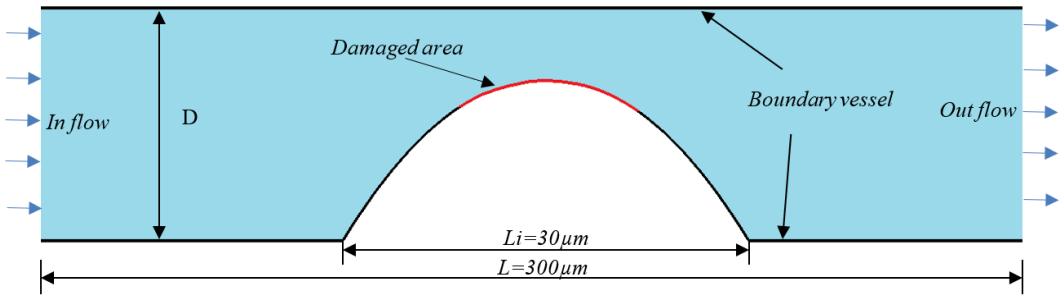

Figure 22: Geomertry of the two-dimentional simulation of a stenosis vessel

Fig. 23 illustrates the growth of the thrombus at various stages (i.e., at 240 s, 320 s, 400 s and 480 s) during the numerical simulation of the blood flow through the stenosed vessel. To demonstrate the effect of aggregation spring constant (K_{ag}), simulations with $K_{ag} = 4.5\text{x}10^9$ N/m (previously used value) and $K_{ag} = 5.0\text{x}10^9$ N/m are presented in Fig. 23. As can be seen from the figure, the growth of the thrombus starts slowly from the upstream side of the damaged area and continues to grow along the downstream of the damaged area where the thrombus grows rapidly in volume. It can be noted from Fig. 23 that a larger amount of thrombus formation occurs near the throat of the stenosis. The results of the numerical simulations also indicate that the thrombus formation nearly results in complete occlusion of the vessel. As the thrombus grows, the flow characteristics changes due to the protruding thrombi, which influences adhesion and aggregation of platelets. Fig. 23 demonstrates that for the modelling parameters chosen in the simulation, the occlusion of the vessel is most likely to occur downstream of the stenosis apex. The presence of stenosis affects haemodynamic of blood flow over the stenosis apex which, in turn may increase platelet activation, as suggested in Karino et al. [Karino and Goldsmith (1979); Lelah and Cooper (1984)]. During the numerical simulation of the stenosed vessel we also observed that the thrombus tends to develop faster than in the case of the straight vessel without stenosis. This is mainly due to the reduction in flow volume across the cross-sectional area. As the flow area is reduced due to the stenosis, more platelets travel in the vicinity of the damaged area. There is thus a rapid growth of thrombus in the case of stenosed vessel. The profile of the thrombus obtained at various stages of the growth compare well with experimental results in literature [Flannery (2005)]. In addition, the number of platelets deposited over the time as demonstrated by Fig. 24 has a similar trend to that of experimental observation noted in Flannery [Flannery (2005)]. The numerical results obtained in the above simulation are promising and may be utilised for predicting valuable information such as location/growth of thrombus and occlusion time.

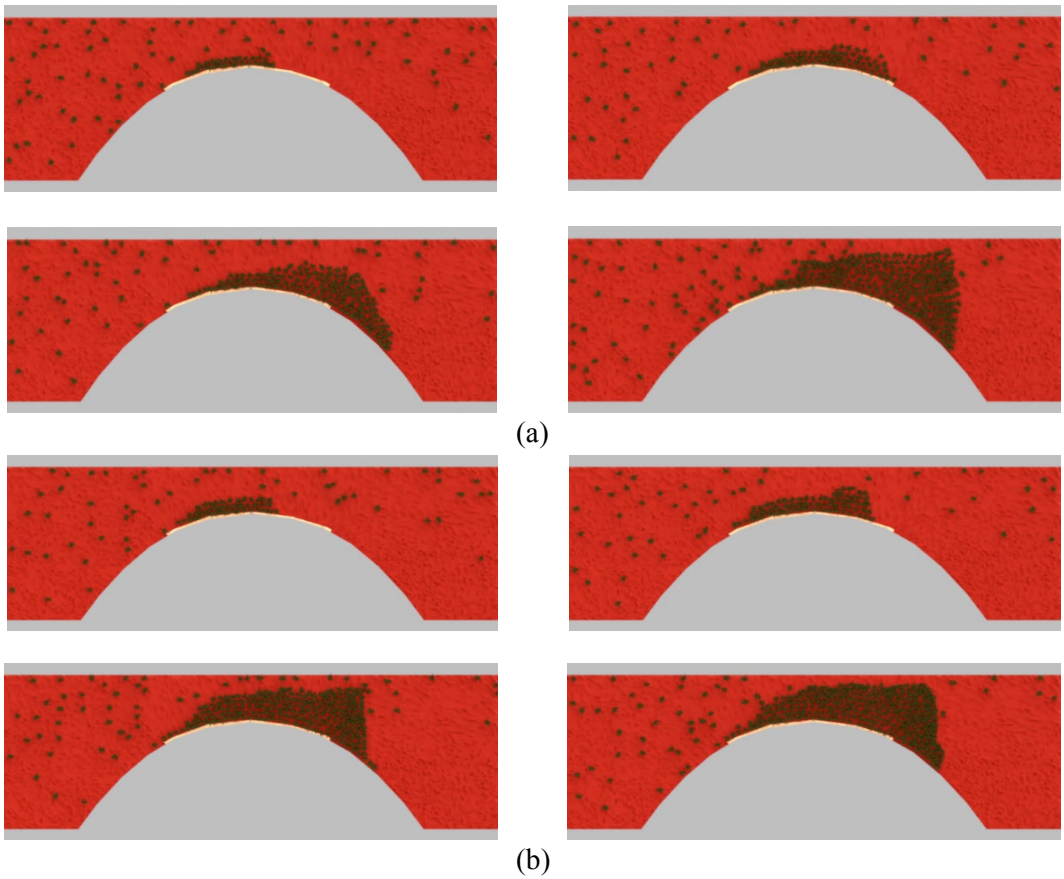

Figure 23: The platelet aggregation for stiffness (a) $K_{ag} = 4.5\text{x}10^9$ N/m; (b) $K_{ag} = 5.0\text{x}10^9$ N/m

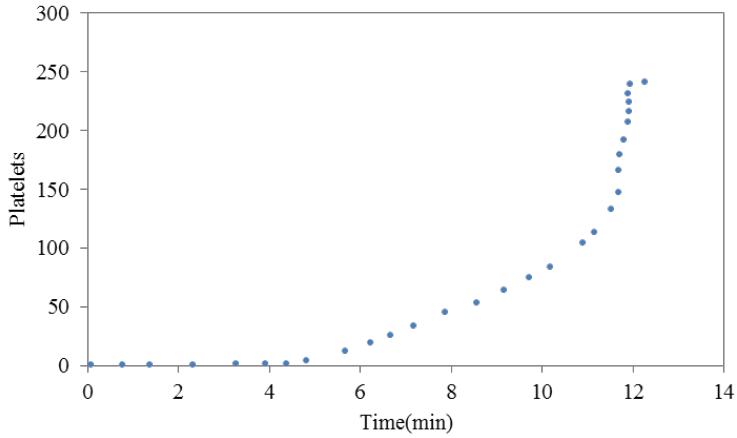

Figure 24: Number of platelets attached and/or aggregated with time

8 Conclusions

This work has focused on the simulation of the thrombogenesis process using the Smooth Particle Hydrodynamics method. The numerical method is developed to model platelets adhesion/aggregation on the surface of damaged area of blood vessels and to investigate the influence of blood flow rates on thrombus growth. In the numerical simulations, blood flow inside vessel is discretised by particles which are assumed to have the characteristics of blood constituents, such as plasma and platelets. The platelet adhesion and aggregation process during the blood flow are modelled by adopting an inter-particle penalty force method. The aforementioned model proved efficient in simulating adhesion and aggregation process without rigorous computational efforts. The potential of the SPH method to simulate thrombogenesis process is demonstrated via a number of numerical examples. The numerical simulations could indicate how blood flow velocity influenced thrombus growth rate in a straight vessel and vessel with bend. The numerical results also qualitatively compare well with experimental observations reported in the literature. This study also demonstrated that the thrombus formation in a stenosis vessel can also be easily modelled using the developed numerical procedures.

It is essential to further investigate the accuracy of the methods developed in a 3-dimensional context. The 3-dimensional simulations will enable the results to be directly and quantitatively compared with the experimental observations reported in Begent et al. [Begent and Born (1970); Flannery (2005)]. In addition, the assumed penalty values (or spring constants) used in the analysis discussed above can be more accurately estimated or calibrated by 3-dimensional numerical models.

Conflicts of Interest: The authors declare that they have no conflicts of interest to report regarding the present study.

References

Amini, Y.; Emdad, H.; Farid, M. (2011): A new model to solve fluid-hypo-elastic solid interaction using the smoothed particle hydrodynamics (SPH) method. *European Journal of Mechanics-B/Fluids*, vol. 30, no. 2, pp. 184-194.

Bark Jr, D. L. (2007): *Mechanistic Numerical Study of Thrombus Growth (M.Sc. Thesis)*. Georgia Institute of Technology, USA.

Batchelor, G. K. (1967): *An Introduction to Fluid Dynamics*. Cambridge University Press, UK.

Begent, N.; Born, G. (1970): Growth rate in vivo of platelet thrombi, produced by iontophoresis of ADP, as a function of mean blood flow velocity. *Nature*, vol. 227, pp. 926-930.

Bonet, J.; Kulasegaram, S. (2000a): Correction and stabilization of smooth particle hydrodynamics methods with applications in metal forming simulations. *International Journal for Numerical Methods in Engineering*, vol. 47, no. 6, pp. 1189-1214.

Bonet, J.; Kulasegaram, S. (2000b): Finite increment gradient stabilization of point integrated meshless methods for elliptic equations. *Communications in Numerical Methods in Engineering*, vol. 16, no. 7, pp. 475-483.

Bonet, J.; Kulasegaram, S. (2002): A simplified approach to enhance the performance of smooth particle hydrodynamics methods. *Applied Mathematics and Computation*, vol. 126, no. 2, pp. 133-155.

Bonet, J.; Lok, T. S. (1999): Variational and momentum preservation aspects of smooth particle hydrodynamic formulations. *Computer Methods in Applied Mechanics and Engineering*, vol. 180, no. 1, pp. 97-115.

Boryczko, K.; Dzwinel, W.; Yuen, D. A. (2003): Dynamical clustering of red blood cells in capillary vessels. *Journal of Molecular Modeling*, vol. 9, no. 1, pp. 16-33.

Bouchnita, A.; Volpert, V. (2019): A multiscale model of platelet-fibrin thrombus growth in the flow. *Computers & Fluids*, vol. 184, pp. 10-20.

Broos, K.; Feys, H. B.; De Meyer, S. F.; Vanhoorelbeke, K.; Deckmyn, H. (2011): Platelets at work in primary hemostasis. *Blood Reviews*, vol. 25, no. 4, pp. 155-167.

Cummins, S. J.; Rudman, M. (1999): An SPH projection method. *Journal of Computational Physics*, vol. 152, no. 2, pp. 584-607.

Denham, M.; Patrick, M. A. (1974): Laminar flow over a downstream-facing step in a two-dimensional flow channel. *Transactions of the Institution of Chemical Engineers*, vol. 52, pp. 361-367.

Epstein, F. H.; Fuster, V.; Badimon, L.; Badimon, J. J.; Chesebro, J. H. (1992): The pathogenesis of coronary artery disease and the acute coronary syndromes. *New England Journal of Medicine*, vol. 326, no. 4, pp. 242-250.

Filipovic, N.; Kojic, M.; Tsuda, A. (2008): Modelling thrombosis using dissipative particle dynamics method. *Philosophical Transactions of the Royal Society of London A: Mathematical, Physical and Engineering Sciences*, vol. 366, pp. 3265-3279.

Flannery, C. J. (2005): *Thrombus Formation under High Shear in Arterial Stenotic Flow (M.Sc. Thesis)*. Georgia Institute of Technology, USA.

Fogelson, A. L. (1992): Continuum models of platelet aggregation: formulation and mechanical properties. *SIAM Journal on Applied Mathematics*, vol. 52, no. 4, pp. 1089-1110.

Fogelson, A. L. (1993): Aggregation: mechanical properties and chemically induced phase transitions. *Fluid Dynamics in Biology: Proceedings of an AMS-IMS-SIAM, American Mathematical Society*, vol. 141, pp. 279-290.

Fogelson, A. L.; Guy, R. D. (2008): Immersed-boundary-type models of intravascular platelet aggregation. *Computer Methods in Applied Mechanics and Engineering*, vol. 197, no. 25, pp. 2087-2104.

Fuster, V.; Badimon, L.; Cohen, M.; Ambrose, J. A.; Badimon, J. et al. (1988): Insights into the pathogenesis of acute ischemic syndromes. *Circulation*, vol. 77, no. 6, pp. 1213-1220.

Gijsen, F.; Van de Vosse, F.; Janssen, J. (1999): The influence of the non-Newtonian properties of blood on the flow in large arteries: steady flow in a carotid bifurcation model. *Journal of Biomechanics*, vol. 32, no. 6, pp. 601-608.

Kamada, H.; Tsubota, K. I.; Nakamura, M.; Wada, S.; Ishikawa, T. et al. (2010): A three-dimensional particle simulation of the formation and collapse of a primary

thrombus. *International Journal for Numerical Methods in Biomedical Engineering*, vol. 26, no. 3-4, pp. 488-500.

Karino, T.; Goldsmith, H. (1979): Adhesion of human platelets to collagen on the walls distal to a tubular expansion. *Microvascular Research*, vol. 17, no. 3, pp. 238-262.

Ku, D. N. (1997): Blood flow in arteries. *Annual Review of Fluid Mechanics*, vol. 29, no. 1, pp. 399-434.

Lee, E. S.; Moulinec, C.; Xu, R.; Violeau, D.; Laurence, D. et al. (2008): Comparisons of weakly compressible and truly incompressible algorithms for the SPH mesh free particle method. *Journal of Computational Physics*, vol. 227, no. 18, pp. 8417-8436.

Lelah, M. D.; Lambrecht, L. K.; Cooper, S. L. (1984): A canine ex vivo series shunt for evaluating thrombus deposition on polymer surfaces. *Journal of Biomedical Materials Research*, vol. 18, no. 5, pp. 475-496.

Merten, M.; Chow, T.; Hellums, J. D.; Thiagarajan, P. (2000): A new role for P-selectin in shear-induced platelet aggregation. *Circulation*, vol. 102, no. 17, pp. 2045-2050.

Miyazaki, H.; Yamaguchi, T. (2002): Formation and destruction of primary thrombi under the influence of blood flow and von Willebrand factor analyzed by a discrete element method. *Biorheology*, vol. 40, no. 1-3, pp. 265-272.

Monaghan, J. J. (1994): Simulating free surface flows with SPH. *Journal of Computational Physics*, vol. 110, no. 2, pp. 399-406.

Morris, J. P.; Fox, P. J.; Zhu, Y. (1997): Modeling low Reynolds number incompressible flows using SPH. *Journal of Computational Physics*, vol. 136, no. 1, pp. 214-226.

Müller, K. (2015): *In Silico Particle Margination in Blood Flow (Ph.D. Thesis)*. Universität zu Köln, Germany.

Nuyttens, B. P.; Thijs, T.; Deckmyn, H.; Broos, K. (2011): Platelet adhesion to collagen. *Thrombosis Research*, vol. 127, pp. S26-S29.

Ou, C.; Huang, W.; Yuen, M. M. (2017): A computational model based on fibrin accumulation for the prediction of stasis thrombosis following flow-diverting treatment in cerebral aneurysms. *Medical & Biological Engineering & Computing*, vol. 55, no. 1, pp. 89-99.

Ouareda, R.; Choparda, B.; Stahla, B.; Rüfenachtb, D. A.; Yilmazb, H. et al. (2008): Thrombosis modeling in intracranial aneurysms: a lattice Boltzmannnumerical algorithm. *Computer Physics Communications*, vol. 179, pp. 128-131.

Panteleev, M.; Sveshnikova, A.; Belyaev, A.; Nechipurenko, D.; Gudich, I. et al. (2014): Systems biology and systems pharmacology of thrombosis. *Mathematical Modelling of Natural Phenomena*, vol. 9, no. 6, pp. 4-16.

Peach, T. W.; Ngoepe, M.; Spranger, K.; Zajarias-Fainsod, D.; Ventiko, Y. (2014): Personalizing flow-diverter intervention for cerebral aneurysms: from computational hemodynamics to biochemical modeling. *International Journal for Numerical Methods in Biomedical Engineering*, vol. 30, pp. 1387-1407.

Rayz, V.; Boussel, L.; Ge, L.; Leach J. R.; Martin A. J. et al. (2010): Flow residence time and regions of intraluminal thrombus deposition in intracranial aneurysms. *Annals of Biomedical Engineering*, vol. 38, no. 10, pp. 3058-3069.

Reininger, A. (2008): Function of von Willebrand factor in haemostasis and thrombosis. *Haemophilia*, vol. 14, no. s5, pp. 11-26.

Robert, A.; Dalrymple, F. A.; Knio, O. (2000): SPH Modelling of water waves. *Proceedings Coastal Dynamics, Lund*, pp. 779-787.

Ruggeri, Z. (2003): Von Willebrand factor, platelets and endothelial cell interactions. *Journal of Thrombosis and Haemostasis*, vol. 1, no. 7, pp. 1335-1342.

Savage, B.; Saldívar, E.; Ruggeri, Z. M. (1996): Initiation of platelet adhesion by arrest onto fibrinogen or translocation on von Willebrand factor. *Cell*, vol. 84, no. 2, pp. 289-297.

Shao, S.; Lo, E. Y. (2003): Incompressible SPH method for simulating Newtonian and non-Newtonian flows with a free surface. *Advances in Water Resources*, vol. 26, no. 7, pp. 787-800.

Sorensen, E. N.; Burgreen, G. W.; Wagner, W. R.; Antaki, J. F. (1999a): Computational simulation of platelet deposition and activation: I. model development and properties. *Annals of Biomedical Engineering*, vol. 27, no. 4, pp. 436-448.

Sorensen, E. N.; Burgreen, G. W.; Wagner, W. R.; Antaki, J. F. (1999b): Computational simulation of platelet deposition and activation: II. results for poiseuille flow over collagen. *Annals of Biomedical Engineering*, vol. 27, no. 4, pp. 449-458.

Takeda, H.; Miyama, S. M.; Sekiya, M. (1994): Numerical simulation of viscous flow by smoothed particle hydrodynamics. *Progress of Theoretical Physics*, vol. 92, no. 5, pp. 939-960.

Wootton, D. M.; Ku, D. N. (1999): Fluid mechanics of vascular systems, diseases, and thrombosis. *Annual Review of Biomedical Engineering*, vol. 1, no. 1, pp. 299-329.

Xu, Z.; Chen, N.; Kamocka, M. M.; Rosen, E. D.; Alber, M. (2008): A multiscale model of thrombus development. *Journal of the Royal Society Interface*, vol. 5, no. 24, pp. 705-722.

Yazdani, A., Li, H., Humphrey, J. D., Karniadakis, G. E. (2017): A general shear dependent model for thrombus formation. *PLoS Computational Biology*, vol. 13, no. 1, e1005291.

Ye, T.; Shi, H.; Phan-Thien, N.; Lim, C. T. (2019): The key events of thrombus formation: platelet adhesion and aggregation. *Biomechanics and Model in Mechanobiology*, pp. 1-13.

Yesudasan, S.; Averett, R. D. (2019): Recent advances in computational modeling of fibrin clot formation: a review. *Computational Biology and Chemistry*, vol. 83, pp. 107-148.